on by climate changes and allowed them to coalesce, potentially leading to the eventual regime shifts and collapses observed in megafaunal ecosystems. The lack of evidence for larger-scale ecological regime shifts during earlier periods of the Glacial (i.e., >45 ka) when interstadial events were common, but modern humans were not, supports a synergistic role for humans in exacerbating the impacts of climate change and extinction in the terminal Pleistocene events.

REFERENCES AND NOTES

1. G. Haynes, *Quat. Int.* **285**, 89–98 (2013).
2. R. D. Guthrie, *Nature* **441**, 207–209 (2006).
3. P. L. Koch, A. D. Barnosky, *Annu. Rev. Ecol. Evol. Syst.* **37**, 215–250 (2006).
4. A. J. Stuart, A. M. Lister, *Quat. Sci. Rev.* **51**, 1–17 (2012).
5. G. Cuvier, Notice sur le squellette d'une très grande espèce de quadrupède inconnue jusqu'à présent, trouvé au Paraguay, et déposé au cabinet d'histoire naturelle de Madrid. *Magasin* encyclopédique, ou *Journal des Sciences, des Lettres et des Arts*, vol. 1, pp. 303–310 and vol. 2, pp. 227–228 (1796).
6. P. S. Martin, in *Quaternary Extinctions: A Prehistoric Revolution*, P. S. Martin, R. D. Klein, Eds. (Univ. of Arizona Press, Tucson, AZ, 1984).
7. J. Diamond, *J. Archaeol. Sci.* **16**, 167–175 (1989).
8. J. Alroy, *Science* **292**, 1893–1896 (2001).
9. E. D. Lorenzen *et al.*, *Nature* **479**, 359–364 (2011).
10. I. Barnes, P. Matheus, B. Shapiro, D. Jensen, A. Cooper, *Science* **295**, 2267–2270 (2002).
11. M. Bunce *et al.*, *Nature* **425**, 172–175 (2003).
12. B. Shapiro *et al.*, *Science* **306**, 1561–1565 (2004).
13. M. Hofreiter, J. Stewart, *Curr. Biol.* **19**, R584–R594 (2009).
14. W. Miller *et al.*, *Proc. Natl. Acad. Sci. U.S.A.* **109**, E2382–E2390 (2012).
15. S. Brace *et al.*, *Proc. Natl. Acad. Sci. U.S.A.* **109**, 20532–20536 (2012).
16. E. W. Wolff, J. Chappellaz, T. Blunier, S. O. Rasmussen, A. Svensson, *Quat. Sci. Rev.* **29**, 2828–2838 (2010).
17. G. Bond *et al.*, *Nature* **365**, 143–147 (1993).
18. S. O. Rasmussen *et al.*, *J. Geophys. Res.* **111**, D06102 (2006).
19. A. Svensson *et al.*, *Clim. Past* **4**, 47–57 (2008).
20. See supplementary materials available on *Science* Online.
21. T. Mourier, S. Y. Ho, M. T. Gilbert, E. Willerslev, L. Orlando, *Mol. Biol. Evol.* **29**, 2241–2251 (2012).
22. G. M. MacDonald *et al.*, *Nat. Commun.* **3**, 893 (2012).
23. R. Muscheler, F. Adolphi, A. Svensson, *Earth Planet. Sci. Lett.* **394**, 209–215 (2014).
24. C. Buizert *et al.*, *Clim. Past* **11**, 153–173 (2015).
25. N. J. Shackleton, R. G. Fairbanks, T. C. Chiu, F. Parrenin, *Quat. Sci. Rev.* **23**, 1513–1522 (2004).
26. J. T. Overpeck, L. C. Peterson, N. Kipp, J. Imbrie, D. Rind, *Nature* **338**, 553–557 (1989).
27. K. A. Hughen, J. T. Overpeck, L. C. Peterson, S. Trumbore, *Nature* **380**, 51–54 (1996).
28. K. Hughen, J. Southon, S. Lehman, C. Bertrand, J. Turnbull, *Quat. Sci. Rev.* **25**, 3216–3227 (2006).
29. L. C. Peterson, G. H. Haug, K. A. Hughen, U. Röhl, *Science* **290**, 1947–1951 (2000).
30. S. C. Porter, A. Zhisheng, *Nature* **375**, 305–308 (1995).
31. Y. Wang *et al.*, *Nature* **451**, 1090–1093 (2008).
32. K. A. Hughen, J. R. Southon, C. J. H. Bertrand, B. Frantz, P. Zermeño, *Radiocarbon* **46**, 1161–1187 (2004).
33. T. J. Heaton, E. Bard, K. Hughen, *Radiocarbon* **55**, 1975–1997 (2013).
34. C. B. Ramsey, *Radiocarbon* **51**, 337–360 (2009).
35. C. J. A. Bradshaw, A. Cooper, C. S. M. Turney, B. W. Brook, *Quat. Sci. Rev.* **33**, 14–19 (2012).
36. P. J. Reimer *et al.*, *Radiocarbon* **55**, 1869–1887 (2013).
37. X. A. S. Wang *et al.*, *Geophys. Res. Lett.* **34**, L23701 (2007).
38. A. J. Stuart, P. A. Kosintsev, T. F. G. Higham, A. M. Lister, *Nature* **431**, 684–689 (2004).
39. J. R. Stewart, *J. Evol. Biol.* **22**, 2363–2375 (2009).
40. B. Huntley *et al.*, *PLOS ONE* **8**, e61963 (2013).
41. P. C. Tzedakis, K. A. Hughen, I. Cacho, K. Harvati, *Nature* **449**, 206–208 (2007).
42. W. E. N. Austin *et al.*, *Quat. Sci. Rev.* **36**, 154–163 (2012).

ACKNOWLEDGMENTS

We thank the following museums and curators for their generous assistance with samples, advice and encouragement: Canadian Museum of Nature (R. Harington); American Museum of Natural History (R. Tedford); Natural History Museum London (A. Currant); Yukon Heritage Centre (J. Storer and G. Zazula); University of Alaska, Fairbanks (D. Guthrie, C. Gerlach, and P. Matheus), Royal Alberta Museum (J. Burns); Institute of Plant and Animal Ecology, RAS Yekaterinburg (P. Kosintsev and A. Vorobiev); Laboratory of Prehistory, St. Petersburg (V. Doronichev and L. Golovanova); D. Froese; T. Higham; A. Sher; J. Glimmerveen; B. Shapiro; T. Gilbert; E. Willerslev; R. Barnett; Yukon miners (B. and R. Johnson, the Christie family, K. Tatlow, S. and N. Schmidt); L. Dalen and J. Soubrier for data and assistance. This work was supported by NSF NESCENT workshop "Integrating datasets to investigate megafaunal extinction in the late Quaternary." A.C., C.T., B.W.B., and C.J.A.B. were supported by Australian Research Council Federation, Laureate and Future Fellowships. The new GICCO5-Cariaco Basin $\delta^{18}O$ record is provided in (*20*) and also lodged on the Paleoclimatology Database (National Oceanic and Atmospheric Administration dataset ID: noaa-icecore-19015). The previously published radiocarbon data, with original references, is presented in (*20*). A.C. and C.T. conceived and performed research; A.C., C.J.A.B., C.T., and B.W.B. designed methods and performed analysis; A.C. and C.T. wrote the paper with input from all authors.

SUPPLEMENTARY MATERIALS

www.sciencemag.org/content/349/6248/602/suppl/DC1
Materials and Methods
Supplementary Text
Figs. S1 to S8
Tables S1 to S4
References (*43*–*54*)

27 April 2015; accepted 3 July 2015
Published online 23 July 2015
10.1126/science.aac4315

IMMUNODEFICIENCIES

Impairment of immunity to *Candida* and *Mycobacterium* in humans with bi-allelic *RORC* mutations

Satoshi Okada,[1,2]* Janet G. Markle,[1]*† Elissa K. Deenick,[3,4]‡ Federico Mele,[5]‡ Dina Averbuch,[6]‡ Macarena Lagos,[7,8]‡ Mohammed Alzahrani,[9]‡ Saleh Al-Muhsen,[9,10]‡ Rabih Halwani,[10] Cindy S. Ma,[3,4] Natalie Wong,[3] Claire Soudais,[11] Lauren A. Henderson,[12] Hiyam Marzouqa,[13] Jamal Shamma,[13] Marcela Gonzalez,[7] Rubén Martinez-Barricarte,[1] Chizuru Okada,[1] Danielle T. Avery,[3] Daniela Latorre,[5] Caroline Deswarte,[14,15] Fabienne Jabot-Hanin,[14,15] Egidio Torrado,[16]§ Jeffrey Fountain,[16]|| Aziz Belkadi,[14,15] Yuval Itan,[1] Bertrand Boisson,[1] Mélanie Migaud,[14,15] Cecilia S. Lindestam Arlehamn,[17] Alessandro Sette,[17] Sylvain Breton,[18] James McCluskey,[19] Jamie Rossjohn,[20,21,22] Jean-Pierre de Villartay,[23] Despina Moshous,[23,24] Sophie Hambleton,[25] Sylvain Latour,[26] Peter D. Arkwright,[27] Capucine Picard,[1,14,15,24,28] Olivier Lantz,[11] Dan Engelhard,[6] Masao Kobayashi,[2] Laurent Abel,[1,14,15] Andrea M. Cooper,[16]¶ Luigi D. Notarangelo,[12,29]¶ Stéphanie Boisson-Dupuis,[1,14,15]¶ Anne Puel,[1,14,15]¶ Federica Sallusto,[5,30]# Jacinta Bustamante,[1,14,15,28]# Stuart G. Tangye,[3,4]# Jean-Laurent Casanova[1,14,15,24,31]†

Human inborn errors of immunity mediated by the cytokines interleukin-17A and interleukin-17F (IL-17A/F) underlie mucocutaneous candidiasis, whereas inborn errors of interferon-γ (IFN-γ) immunity underlie mycobacterial disease. We report the discovery of bi-allelic *RORC* loss-of-function mutations in seven individuals from three kindreds of different ethnic origins with both candidiasis and mycobacteriosis. The lack of functional RORγ and RORγT isoforms resulted in the absence of IL-17A/F–producing T cells in these individuals, probably accounting for their chronic candidiasis. Unexpectedly, leukocytes from RORγ- and RORγT-deficient individuals also displayed an impaired IFN-γ response to *Mycobacterium*. This principally reflected profoundly defective IFN-γ production by circulating γδ T cells and $CD4^+CCR6^+CXCR3^+$ αβ T cells. In humans, both mucocutaneous immunity to *Candida* and systemic immunity to *Mycobacterium* require RORγ, RORγT, or both.

Inborn errors of human interleukin-17A and interleukin-17F (IL-17A/F) or interferon-γ (IFN-γ) immunity are each associated with a specific set of infections. Inborn errors of IL-17A/F underlie chronic mucocutaneous candidiasis (CMC), which is characterized by infections of the skin, nails, and oral and genital mucosae with *Candida albicans*, typically in the absence of other infections. Five genetic etiologies of CMC have been reported, with mutations in five genes (*1*, *2*). Inborn errors of IFN-γ underlie Mendelian susceptibility to mycobacterial disease (MSMD), which is characterized by selective susceptibility to weakly pathogenic mycobacteria, such as *Mycobacterium bovis* Bacille Calmette-Guérin (BCG) vaccines and environmental mycobacteria. Eighteen genetic etiologies of MSMD have been reported, involving mutations of nine genes (*3*, *4*). Only a few patients display both candidiasis and mycobacteriosis, including some

patients with IL-12p40 and IL-12Rβ1 deficiencies, which impair IFN-γ immunity in all patients and IL-17A/F immunity in some patients (*4*). We studied seven patients from three unrelated consanguineous families with this unusual combination of infectious diseases but no known genetic disorder. A Palestinian child (Fig. 1A, Kindred A, patient P1; see also supplementary text) died at the age of 6 years from disseminated BCG disease. Two other children (P2 and P3) in Kindred A had similar clinical presentations but survived and are now 7 and 4 years old, respectively. A 6-year-old Chilean child (Fig. 1A, Kindred B, P4; see also supplementary text) had disseminated BCG infection at age 16 months. Finally, three siblings from Saudi Arabia (Fig. 1A, Kindred C, P5, P6, and P7; see also supplementary text), ages 9, 6, and 3 years, had mycobacterial diseases caused by BCG in two children and by *M. tuberculosis* in the third. Six of the seven patients also had mucocutaneous candidiasis of varying severity (table S1).

Bi-allelic *RORC* mutations

We combined whole-exome sequencing and genome-wide linkage (GWL) analysis to search for homozygous genetic lesions in the three probands (P1, P4, and P6) (fig. S1). We identified a homozygous C/T mutation in the *RORC* gene in P1, P2, and P3, resulting in a missense Ser^{38}→Leu^{38} (S38L) substitution in the RORγ isoform or a S17L substitution in the RORγT isoform (Fig. 1, A and B, and fig. S2). In P4, we identified a homozygous *RORC* C/T mutation converting the Gln^{329} (Q329) residue of RORγ (or Q308 in RORγT) into a stop codon (Fig. 1, A and B, and fig. S2). In P5, P6, and P7, we identified a homozygous C/T mutation converting the Q441 residue of RORγ (or Q420 in RORγT) into a stop codon (Fig. 1, A and B, and fig. S2). In each kindred, all unaffected family members were either heterozygous or homozygous for the wild-type (WT) allele (Fig. 1A and fig. S2). The familial segregation of these mutant *RORC* alleles was therefore consistent with an autosomal recessive (AR) pattern of inheritance. There were no other genes mutated in the three kindreds among the 173 genes on the 6.87-Mb interval linked with disease (maximum LOD score 6.35). The S17L mutation affects a strictly conserved residue of the DNA binding domain of RORγT (Fig. 1B) and is predicted to be damaging by multiple software algorithms (*5*). The Q308X and Q420X (X signifies a stop codon) nonsense mutations are predicted to result in truncated proteins lacking part of the ligand-binding domain (Fig. 1B). The Q308X and Q420X alleles were not found in the National Center for Biotechnology Information, Ensembl, Exome Aggregation Consortium (ExAC), and dbSNP databases; in our own in-house database of more than 3000 exomes; or in 1052 controls from 52 ethnic groups in the CEPH-HGD panel, indicating that they were very rare variants, possibly exclusive to these two kindreds. There were no nonsense or frameshift mutations affecting isoform 2 (RORγT) in these databases. The S17L allele was found in one heterozygous individual of the ExAC database, indicating that its frequency is less than 10^{-5}. We therefore hypothesized that the bi-allelic *RORC* mutations found in these three kindreds were disease-causing.

Complete RORγ and RORγT deficiency

In mice and humans, the RORγ and RORγT isoforms are generated by transcription from different start sites (*6*–*10*) (Fig. 1B). Both molecules are transcription factors, but they have different expression patterns in inbred mice: RORγ is ubiquitous, whereas RORγT is restricted to leukocytes (*10*). RORγT plays an important role in T cell development and function in mice (*11*, *12*). Animals lacking only RORγT apparently have the same immunological phenotype as those lacking both isoforms (*10*). We first assessed the effect of *RORC* mutations by transiently expressing WT and mutant RORγT and RORγ in human embryonic kidney 293T (HEK293T) cells in the presence and absence of stimulation with phorbol 12-myristate 13-acetate (PMA) and ionomycin. We detected both the WT and S17L RORγT proteins at the expected molecular mass of 56 kD (Fig. 1C). The Q308X and Q420X RORγT mutant proteins had molecular weights consistent with truncation at residues 308 and 420, respectively (Fig. 1C). Similar results were obtained upon expression of RORγ (fig. S3). We then performed an electrophoretic mobility shift assay (EMSA) to assess the ability of the mutant RORγT and RORγ isoforms to respectively bind to RORE-2 and RORE-1, the consensus binding sites in the promoter of *IL17A* (fig. S3). The three mutations abolished DNA binding of RORγT to RORE-2 (Fig. 1C) and of RORγ to RORE-1 (fig. S3), but not by disrupting the nuclear localization of the protein (fig. S3). Each mutation resulted in the loss of *IL17A* promoter activation by RORγT (Fig. 1D) or RORγ (fig. S4). Thus, each mutant allele was associated with a complete loss of function of the two encoded protein isoforms, identifying these patients as cases of human AR complete RORγ/RORγT deficiency (hereafter referred to as RORγT deficiency).

Broad immunological phenotype

Mouse RORγT is expressed in lymphoid tissue inducer (LTi) cells, type 3 innate lymphoid cells (ILC3), type 1 natural killer T (NKT) cells, some γδ T cells, immature $CD4^+CD8^+$ αβ thymocytes, and IL-17A/F–producing $CD4^+$ αβ T cells [T helper 17 (T_H17) cells] (*7*, *11*, *13*–*16*). LTi, ILC3, type 1 NKT, and T_H17 cells fail to develop in $Rorc^{-/-}$ mice, and $CD4^+CD8^+$ αβ thymocytes have a reduced life span (*11*, *14*, *17*). $RORC^{-/-}$ patients displayed clinical signs consistent with LTi deficiency, including absence of palpable axillary and cervical lymph nodes (despite visible tonsils), and had reduced thymus size (Fig. 2A). As in $Rorc^{-/-}$ mice, ILC3 were barely detectable in the patients' blood (fig. S5). In $Rorc^{-/-}$ mice, the short life span of $CD4^+CD8^+$ αβ thymocytes results in an inability to use the most 5′ segments of the T cell receptor (TCR) Vα array (*12*), including those encoding the Vα chains of mucosal associated invariant T (MAIT) (*12*) and type 1 NKT cells (*18*). High-throughput sequencing of the *TRA/TRD* and *TRG* loci revealed that 5′ Vα gene segment use had decreased, whereas Vδ and Vγ usage was normal in $RORC^{-/-}$ T cell clonotypes (fig. S6). Further, these patients lacked *TRA* clonotypes using 5′ Vα and distal 3′ Jα pairings (fig. S6). In total $RORC^{-/-}$ T cell clonotypes, the usage of Vγ9 was elevated (fig. S6), consistent with antigen-driven peripheral expansion of this subset, perhaps driven by mycobacteria (*19*). Abolished use of the Vα segments *TRAV10* (encoding Vα24) and *TRAV1.2* (encoding Vα7.2) was confirmed by quantitative polymerase chain reaction

[1]St. Giles Laboratory of Human Genetics of Infectious Diseases, Rockefeller Branch, The Rockefeller University, New York, NY 10065, USA. [2]Department of Pediatrics, Hiroshima University Graduate School of Biomedical and Health Sciences, Hiroshima, Japan. [3]Immunology Division, Garvan Institute of Medical Research, Darlinghurst, New South Wales, Australia. [4]St Vincent's Clinical School, University of New South Wales, Sydney, New South Wales, Australia. [5]Institute for Research in Biomedicine, University of Italian Switzerland, Bellinzona, Switzerland. [6]Department of Pediatrics, Hadassah University Hospital, Jerusalem, Israel. [7]Department of Immunology, School of Medicine, Universidad de Valparaíso, Santiago, Chile. [8]Department of Pediatrics, Padre Hurtado Hospital and Clinica Alemana, Santiago, Chile. [9]Department of Pediatrics, King Faisal Specialist Hospital and Research Center, Riyadh, Saudi Arabia. [10]Department of Pediatrics, Prince Naif Center for Immunology Research, College of Medicine, King Saud University, Riyadh, Saudi Arabia. [11]Institut Curie, INSERM U932, Paris, France. [12]Division of Immunology, Boston Children's Hospital, Boston, MA 02115, USA. [13]Caritas Baby Hospital, Post Office Box 11535, Jerusalem, Israel. [14]Laboratory of Human Genetics of Infectious Diseases, Necker Branch, INSERM UMR 1163, Paris, France. [15]Paris Descartes University, Imagine Institute, Paris, France. [16]Trudeau Institute, Saranac Lake, NY 12983, USA. [17]La Jolla Institute for Allergy and Immunology, La Jolla, CA 92037, USA. [18]Department of Radiology, Assistance Publique–Hôpitaux de Paris (AP-HP), Necker Hospital for Sick Children, Paris, France. [19]Department of Microbiology and Immunology, Peter Doherty Institute for Infection and Immunity, University of Melbourne, Parkville, Victoria, Australia. [20]Department of Biochemistry and Molecular Biology, School of Biomedical Sciences, Monash University, Clayton, Victoria, Australia. [21]Australian Research Council Centre of Excellence for Advanced Molecular Imaging, Monash University, Clayton, Victoria, Australia. [22]Institute of Infection and Immunity, Cardiff University, School of Medicine, Heath Park, Cardiff CF14 4XN, UK. [23]Laboratoire Dynamique du Génome et Système Immunitaire, INSERM UMR 1163, Université Paris Descartes–Sorbonne Paris Cité, Imagine Institute, Paris, France. [24]Pediatric Hematology-Immunology Unit, AP-HP, Necker Hospital for Sick Children, Paris, France. [25]Institute of Cellular Medicine, Newcastle University and Great North Children's Hospital, Newcastle upon Tyne NE4 6BE, UK. [26]Laboratory of Lymphocyte Activation and Susceptibility to EBV Infection, INSERM UMR 1163, Université Paris Descartes–Sorbonne Paris Cité, Imagine Institute, Paris, France. [27]Department of Paediatric Allergy Immunology, University of Manchester, Royal Manchester Children's Hospital, Manchester, UK. [28]Center for the Study of Primary Immunodeficiencies, AP-HP, Necker Hospital for Sick Children, Paris, France. [29]Manton Center for Orphan Disease Research, Children's Hospital, Boston, MA 02115, USA. [30]Center of Medical Immunology, Institute for Research in Biomedicine, University of Italian Switzerland, Bellinzona, Switzerland. [31]Howard Hughes Medical Institute, New York, NY 10065, USA.

*These authors contributed equally to this work. **†Corresponding author. E-mail: jmarkle@rockefeller.edu (J.G.M.); jean-laurent.casanova@rockefeller.edu (J.-L.C.)** ‡These authors contributed equally to this work. §Present address: Life and Health Sciences Research Institute (ICVS), School of Health Sciences, University of Minho, Braga, Portugal. ||Present address: National Center for HIV/AIDS, Viral Hepatitis, STD, and TB Prevention, Office of Infectious Diseases, Centers for Disease Control and Prevention, Atlanta, GA 30329, USA. ¶These authors contributed equally to this work. #These authors contributed equally to this work.

(fig. S7) and resulted in a lack of both CD161^{+}Vα7.2^{+} MAIT cells and Vα24^{+}Vβ11^{+} type 1 NKT cells (Fig. 2, B and C, and fig. S7). Some Vα7.2^{+} cells other than MAIT cells have recently been shown to recognize *Mycobacterium*-derived mycolyl lipids (*20*); they were also missing in *RORC*$^{-/-}$ patients. Nevertheless, *RORC*$^{-/-}$ patients displayed only mild CD4^{+} and CD8^{+} αβ T cell lymphopenia, with normal B and NK cell counts (Fig. 2D and table S2). These patients did not, therefore, have T cell deficiency [also known as "combined" immunodeficiency (CID)], consistent with their lack of broad infectious and autoimmune phenotypes (*21*). Finally, the frequencies of circulating γδ T cells were normal (table S2). Overall, these *RORC*$^{-/-}$ patients displayed the general immunological features characteristic of *Rorc*$^{-/-}$ mice (*11*, *12*, *14*, *22*, *23*). These studies also revealed that the development of MAIT and other Vα7.2^{+} T cells is critically dependent on RORγT, which had been predicted but not shown in mice. No infectious phenotype can be unambiguously assigned to any of these individual immunological anomalies.

Abolished production of IL-17A/F

Given the critical role of murine RORγT in generating IL-17A/F– and IL-22–producing lymphocytes [including ILC3, γδ T cells, and T_H17 cells (*11*, *13*, *24*)] and the finding that patients with compromised IL-17A/F immunity are susceptible to mucocutaneous candidiasis (*1*), we assessed the development and function of IL-17A/F–producing lymphocytes in the patients. Circulating ILC3 were too few to assess their production of IL-17. CD3^{+} T cells from *RORC*$^{-/-}$ patients displayed a severe impairment in the production of IL-17A, IL-17F, and IL-22, at both the mRNA (fig. S8) and the protein level (Fig. 3A), after polyclonal stimulation. CD4^{+} αβ T cells are a major source of IL-17A/F (*9*). Memory (CD45RA^{-}) CD4^{+} T cells from *RORC*$^{-/-}$ patients produced much less IL-17A, IL-17F, and IL-22 than WT and heterozygous controls (Fig. 3B).

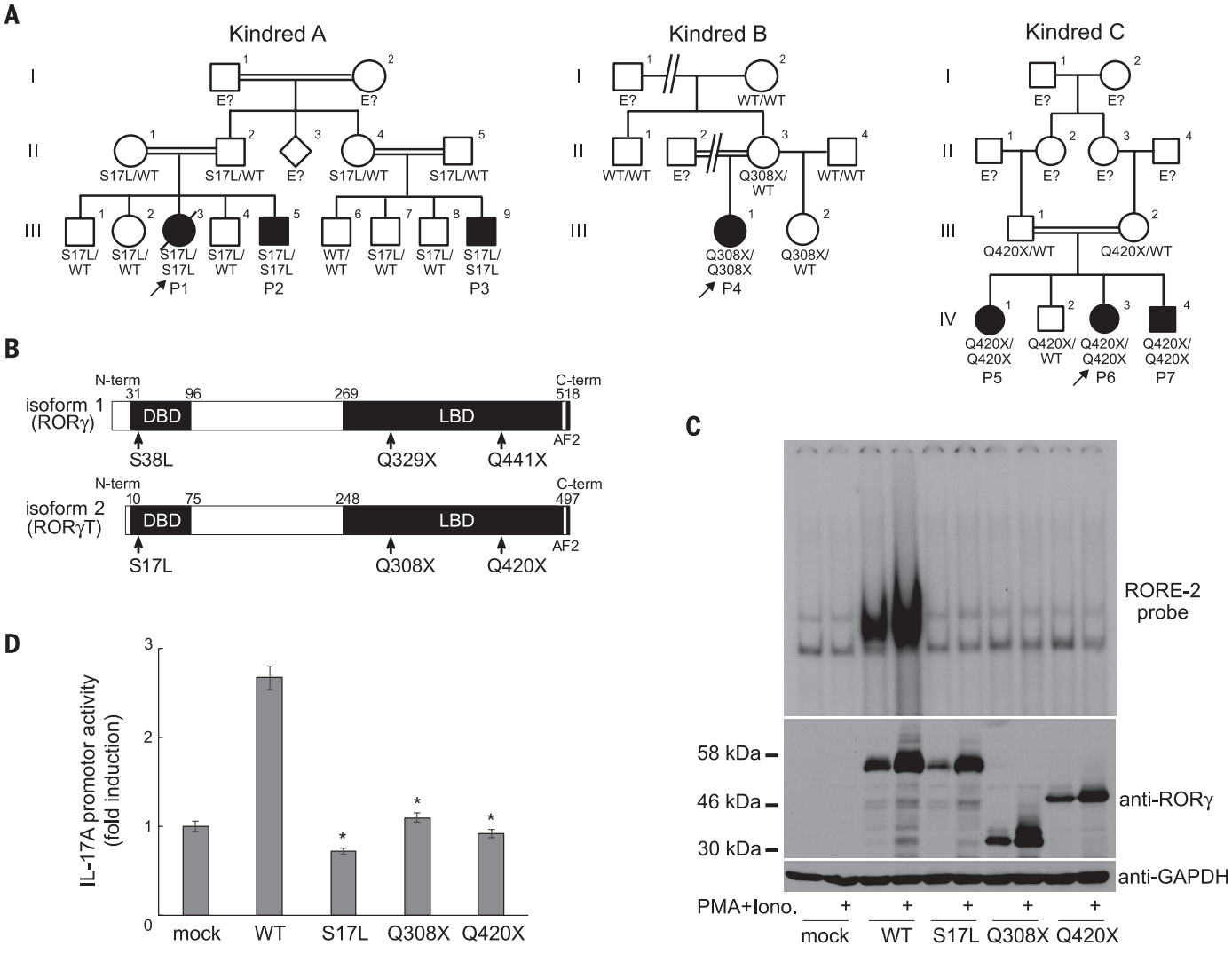

Fig. 1. Identification of homozygous loss-of-function mutations affecting the human RORγT protein. (**A**) Sanger sequencing results and familial segregation of previously unidentified homozygous *RORC* mutations in three unrelated consanguineous families, indicating an AR pattern of inheritance, with complete clinical penetrance. P1, patient 1; P2, patient 2; etc. (**B**) Graphical representation of the RORγ and RORγT proteins, encoded by *RORC* isoforms 1 and 2, respectively. AF2, activation function 2 domain. Arrows indicate the location of the sites affected by the *RORC* mutations found in the families. DBD, DNA binding domain; LBD, ligand-binding domain. (**C**) HEK293T cells were either mock-transfected or transfected with the indicated plasmids. After 24 hours, cells were either left untreated or stimulated with PMA and ionomycin. Whole-cell lysates were obtained and subjected to Western blotting (lower panel), and nuclear lysates were subjected to EMSA with a ^{32}P-labeled RORE-2 probe derived from the *IL17A* promoter sequence (upper panel). GAPDH, glyceraldehyde-3-phosphate dehydrogenase. (**D**) *IL17A* reporter plasmids, the pRL-SV40 vector, and WT or mutant *RORC* plasmid were used to transfect HEK293T cells. After 24 hours, cells were stimulated with PMA and ionomycin as in (C) and then subjected to luciferase assays. Experiments were performed in triplicate, and *IL17A* promoter activity is expressed as fold induction relative to mock-transfected cells. *P < 0.05 versus WT controls; two-tailed Mann-Whitney tests with Bonferroni correction. Error bars denote SEM.

In contrast, the memory $CD4^+$ T cells from these patients produced large amounts of IL-4, IL-5, and IL-13 (fig. S8). In separate experiments, naïve ($CD45RA^+CCR7^+$) $CD4^+$ T cells from *RORC*$^{-/-}$ patients cultured under T_H17-polarizing conditions secreted less IL-17A and IL-17F than cells from healthy donors or heterozygous relatives (Fig. 3C). We next assessed the proliferation and cytokine secretion of highly purified WT, heterozygous, and *RORC*$^{-/-}$ $CD4^+CCR6^+$ memory αβ T cells (fig. S9), a population enriched in IL-17A/F–secreting cells (T_H17 cells, which express CCR4), as well as cells secreting IL-17A/F and IFN-γ (herein designated as T_H1^* cells, which express CXCR3) (*25*), after stimulation with *C. albicans* lysate. By monitoring the incorporation of a radioactive label, we found that $CD4^+CCR6^+$ T cells from *RORC*$^{-/-}$ patients had normal frequencies of antigen-specific cells recognizing *C. albicans* (Fig. 3D). However, these cells [including both T_H17 and T_H1^* cells, whose proportions were normal (fig. S9)] secreted much lower amounts of IL-17A and IL-22 than did control cells (Fig. 3E). IFN-γ was also reduced, but large amounts of IL-4 were secreted, serving as a control (Fig. 3E). Finally, *Herpesvirus saimiri*–transformed $CD4^+$ αβ T cells from *RORC*$^{-/-}$ patients showed abolished induction of *RORC* (Fig. 4A) and *IL17A* (Fig. 4B), but not *IFNG* serving as a control (fig. S10). The defect in *IL17A* induction could be rescued by retroviral transduction with WT *RORC* (Fig. 4B). Collectively, these data demonstrate a profound diminution of IL-17A/F and IL-22 production by all leukocytes tested in *RORC*$^{-/-}$ patients. As CMC-causing germline mutations have previously been identified in *IL17F*, *IL17RA*, *IL17RC*, and *ACT1* (*1*, *2*, *26*), we conclude that impaired IL-17A/F immunity in *RORC*$^{-/-}$ patients accounts for their development of CMC. Human IL-17A/F–producing ILC3, γδ T cells, and αβ T cells, or any of their subsets, may individually or collectively confer protection against *Candida*.

Selective defect in IFN-γ production

We then investigated the cellular mechanism underlying the patients' surprising susceptibility to mycobacteria. The patients did not display chronic granulomatous disease or severe CID, which can underlie BCG disease (*4*). The $CD3^+$ T cells (including both γδ and αβ T cells) from *RORC*$^{-/-}$ patients produced IFN-γ normally, after the stimulation of whole blood or peripheral blood mononuclear cells (PBMCs) with PMA and ionomycin (fig. S10). Likewise, total $CD4^+$ αβ T cells, memory ($CD45RA^-$) $CD4^+$ T cells, naïve $CD4^+$ T cells cultured under T_H1-polarizing conditions, and *Herpesvirus saimiri*–transformed T cells from

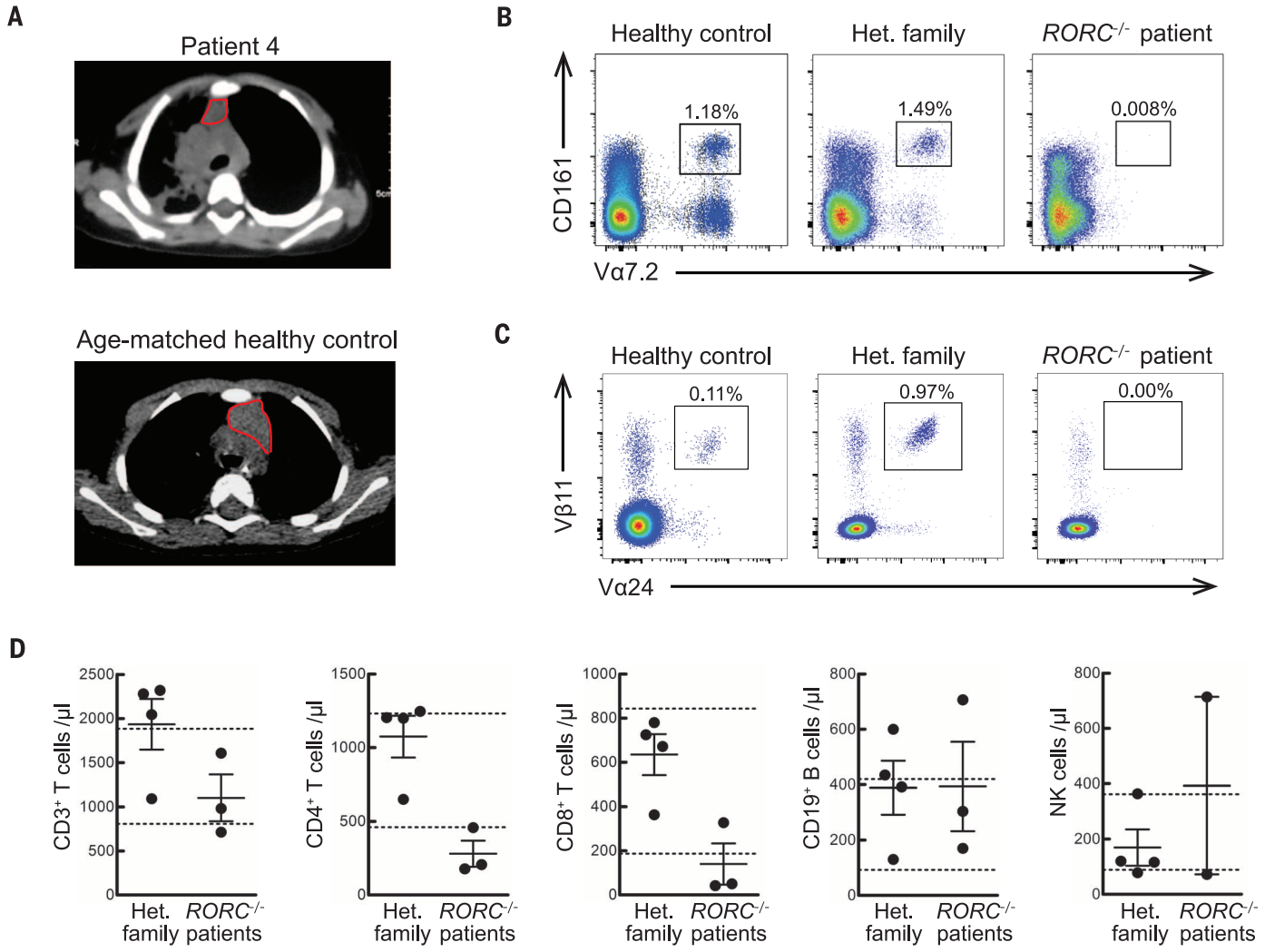

Fig. 2. *RORC*$^{-/-}$ patients display abnormal thymus size and TCRα rearrangement in line with their mild T cell lymphopenia with a complete absence of MAIT and type 1 NKT cells. (**A**) Computed tomography (CT) scan of P4's chest at the age of 16 months compared with a CT scan of a healthy control. P4's scan reveals right lung infiltrate and thymic hypoplasia. (**B** and **C**) PBMCs from WT controls, heterozygous family members, or *RORC*$^{-/-}$ patients were analyzed for MAIT (B) and type 1 NKT (C) cell frequencies by flow cytometry. Each plot is representative of $n = 3$ experiments. (**D**) Cell counts were performed on fresh blood samples from heterozygous family members ($n = 4$) and *RORC*$^{-/-}$ patients ($n = 3$). Dotted lines indicate the normal ranges for each lymphocyte population per microliter of blood, based on the results for healthy individuals tested at the Necker Hospital for Sick Children (Paris, France).

the patients produced IFN-γ normally (fig. S10). Overall, and in contrast to the IL-17A/F defect, RORγT deficiency does not impair IFN-γ secretion in conditions of polyclonal stimulation. We next assessed *Mycobacterium*-specific IFN-γ responses from whole blood (Fig. 5A) or PBMCs (Fig. 5B) of *RORC*$^{-/-}$ patients, heterozygous family members, and healthy controls. The patients' cells produced very little IFN-γ in response to treatment with BCG plus IL-12 (Fig. 5, A and B). This defect was as profound as that seen in patients with IL-12Rβ1 deficiency (*27*). The production of IL-12p40 by *RORC*$^{-/-}$ cells was normal (fig. S11). Impaired IFN-γ production may account for mycobacterial diseases in *RORC*$^{-/-}$ patients. This IFN-γ defect was not secondary to excessive IL-4, IL-5, or IL-13 production (fig. S11) or to the IL-17A/F defect (fig. S12). Many single-gene immunodeficiencies do not predispose to BCG disease despite impaired or abolished development or function of various αβ T cell subsets, including CD4$^+$ T cells (*28*), CD8$^+$ T cells (*29*), type 1 NKT cells (*30*, *31*), and MAIT cells (*31*). Even rare patients deficient in total αβ T cell function [*ZAP70*$^{-/-}$ (*32*), *TRAC*$^{-/-}$ (*33*)] have not been reported to develop BCG disease. Whole blood or PBMCs from such patients responded normally to treatment with BCG plus IL-12, except for patients lacking all functional αβ T cells (fig. S12). As MAIT cells were shown to respond to mycobacteria (*34*), we purified these

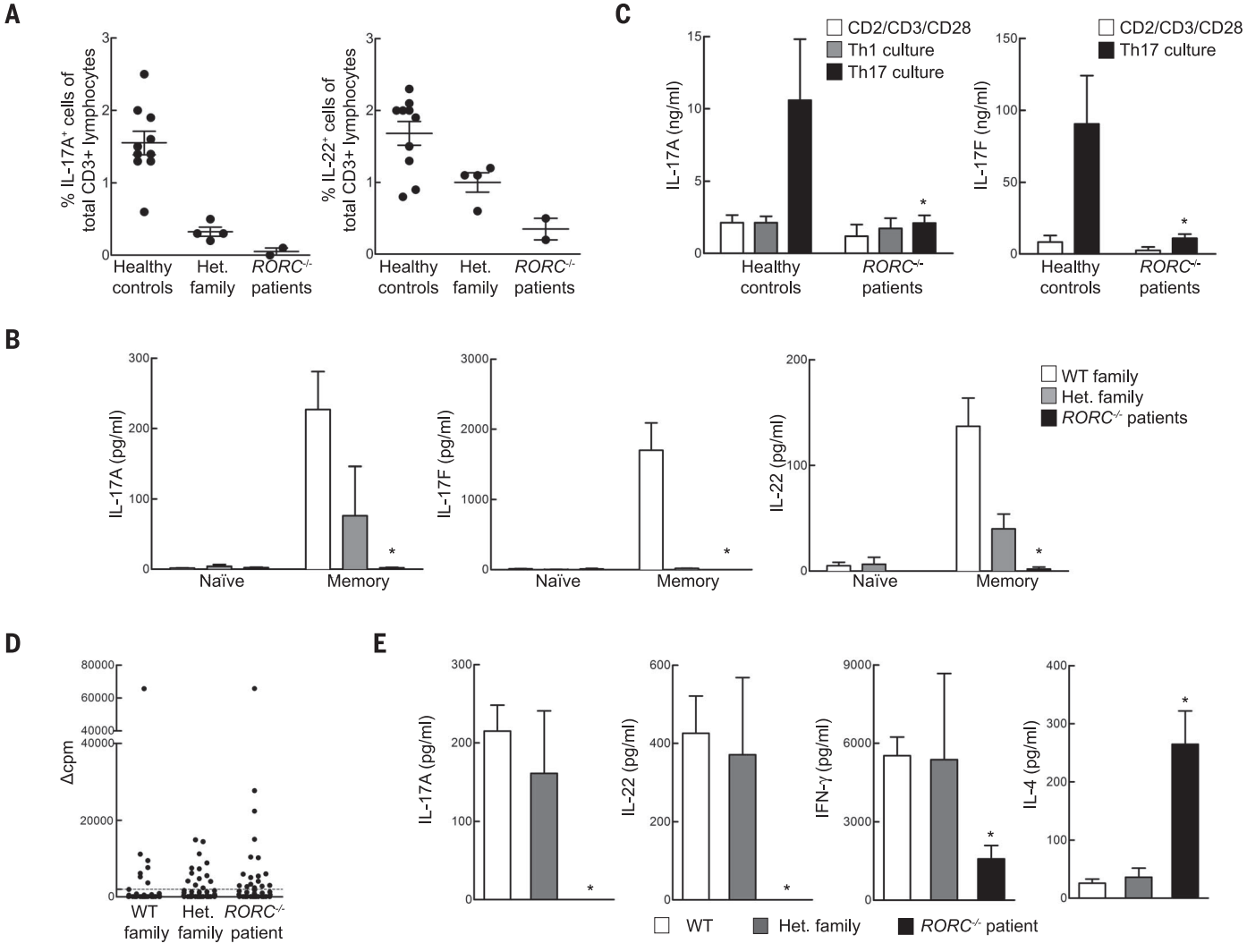

Fig. 3. Cellular mechanisms of compromised IL-17 immunity and CMC in *RORC*$^{-/-}$ patients. (**A**) Whole blood from healthy WT donors, heterozygous family members, or *RORC*$^{-/-}$ patients was activated by PMA and ionomycin in the presence of brefeldin A, then assessed by intracellular flow cytometry for the production of IL-17A and IL-22. (**B**) Naïve and memory CD4$^+$ T cells from WT controls (n = 7), heterozygous family members (n = 2), and *RORC*$^{-/-}$ patients (n = 3) were cultured with T cell activation and expansion (TAE) beads, and the culture supernatants were then assessed for secretion of the cytokine indicated (*37*). (**C**) Cytokine production by in vitro–differentiated CD4$^+$ T cells from control donors and *RORC*$^{-/-}$ patients. Naïve (CD45RA$^+$CCR7$^+$) CD4$^+$ T cells were purified from the PBMCs of WT controls (n = 6) or *RORC*$^{-/-}$ patients (n = 3), then cultured in the presence of TAE beads alone or TAE beads together with polarizing stimuli to induce the differentiation of T_H1- or T_H17-type cells (*37*). After 5 days, culture supernatants were assessed for the secretion of the cytokines indicated. (**D**) Sorted CCR6$^+$ memory CD4$^+$ T cells from WT controls, heterozygous family members, and *RORC*$^{-/-}$ patients were initially polyclonally stimulated to generate T cell libraries, then cultured with autologous irradiated B cells, with or without a 3-hour pulse with *C. albicans* lysate (5 μg/ml) (*37*). Proliferation was assessed by evaluating radiolabel incorporation on day 4 and is expressed as Δcpm values (cpm, counts per minute) (*37*). Dotted lines represent the cutoff values. The frequencies of specific T cells using the Poisson distribution were 315/10^6, 631/10^6, and 874/10^6 in WT control, heterozygous family member, and *RORC*$^{-/-}$ patient, respectively. (**E**) Concentrations of the indicated cytokines were measured in the supernatants from positive cultures (Δcpm values above the cut-off value) from experiments performed as in (D) with cells from WT controls, heterozygous family members, and *RORC*$^{-/-}$ patients (n = 2 each). Number of wells: n = 45 to 64 for WT controls, n = 4 to 10 for heterozygous family members, and n = 14 to 23 for *RORC*$^{-/-}$ patients. *P < 0.05 versus WT controls; in two-tailed Mann-Whitney tests with Bonferroni correction. Error bars in (B), (C), and (E) indicate SEM.

cells from WT donor PBMCs and added them to PBMCs from *RORC*$^{-/-}$ patients before BCG stimulation. The lack of MAIT cells in *RORC*$^{-/-}$ patients did not account for their impaired IFN-γ production (fig. S13). Overall, the absence of type 1 NKT and MAIT cells, the mild T cell lymphopenia, and the poor development of IL-17A/F T cells may contribute marginally to mycobacterial susceptibility but do not account for the low level of IFN-γ production by *RORC*$^{-/-}$ leukocytes stimulated with BCG and IL-12, and probably not for the patients' mycobacterial disease.

Impaired IFN-γ production by γδ T cells

We thus systematically characterized the consequences of leukocyte population depletions on BCG-dependent IFN-γ production by PBMCs in healthy controls. We found no overt IFN-γ defect as a consequence of depleting NK cells, CD14$^+$ cells, or CD4$^+$ or CD8$^+$ T cells. Depletion of αβ T cells, γδ T cells, or both resulted in diminished IFN-γ production (fig. S14). To probe the kinetics of this phenotype, a similar experiment was repeated and supernatant was assessed at 6, 12, 18, 24, and 48 hours poststimulation (fig. S14). The effect of γδ T cell depletion was most apparent at 24 hours (fig. S14). We observed high expression of *RORC* isoform 2 mRNA in both αβ and γδ T cells of healthy donors (fig. S15), prompting further analyses of γδ T cell function. Flow cytometry analyses revealed that the TCR^{high} γδ T cells from *RORC*$^{-/-}$ patients could not secrete IFN-γ in response to stimulation with PMA and ionomycin, unlike TCR^{low} γδ T cells (fig. S15). TCR Vδ2$^+$ cells have been reported as the predominant cells responding to human BCG vaccination (*19*). *RORC*$^{-/-}$ patients had normal frequencies of TCR Vδ2$^+$ cells, but these cells were unable to secrete IFN-γ when stimulated with PMA and ionomycin (fig. S15), suggesting a possible contribution of this γδ T cell subset defect to mycobacterial susceptibility in *RORC*$^{-/-}$ patients. Overall, RORγT deficiency diminishes the IFN-γ–producing capacity of γδ T cells, which normally produce this cytokine in response to *Mycobacterium* stimulation.

The patients' CD4$^+$CCR6$^+$ αβ T cells produce little IFN-γ in response to BCG

Previous studies have demonstrated that the T-bet– and RORγT-expressing, IFN-γ and IL-17A/F–producing CCR6$^+$CXCR3$^+$ T$_H$1* subset is strongly enriched for *Mycobacterium*-responsive CD4$^+$ αβ T cells, unlike the CCR6$^+$CCR4$^+$ T$_H$17 cells that only express RORγT and produce IL-17A/F and are enriched for *Candida*-responsive T cells (*25*). We therefore purified memory (CD45RA$^-$) αβ T cell subsets (fig. S9) and assessed their proliferation and cytokine production in response to a pool of BCG peptides. CD4$^+$CCR6$^+$ αβ T cells from *RORC*$^{-/-}$ patients had a normal or high frequency of antigen-specific cells recognizing BCG peptides, as demonstrated by the induction of proliferation (Fig. 5C and fig. S16). However, although CD4$^+$CCR6$^+$ T cells from *RORC*$^{-/-}$ patients responded to mycobacterial antigens, they secreted much less IFN-γ than CD4$^+$CCR6$^+$ αβ T cells from normal donors (Fig. 5D). The normal proliferation and cytokine production of other CD4$^+$ memory T cell subsets in response to *Candida* and *Mycobacterium* (fig. S17) and to irrelevant viral stimuli (fig. S18) indicate a selective RORγT-dependent functional defect in *Mycobacterium*-specific CD4$^+$CCR6$^+$ αβ T cells. Although we did not purify and test T$_H$1* cells, they were present in normal proportions in the patients (fig. S9), implying that they are functionally defective for IFN-γ production upon *Mycobacterium* stimulation. Collectively, these data suggest that mycobacterial diseases in *RORC*$^{-/-}$ patients may result from the poor production of IFN-γ by γδ T cells, CCR6$^+$CXCR3$^+$CD4$^+$ αβ T$_H$1* cells, or both in response to mycobacteria. IFN-γ treatment may therefore be beneficial for *RORC*$^{-/-}$ patients. This combined defect probably also accounts for mycobacterial disease in severe combined immunodeficient patients, as patients with various forms of CID are normally resistant to BCG (*27*, *33*). Finally, the lack of MAIT and type 1 NKT cells, reduction in ILC3, and possibly the absence of other lymphocytes not analyzed using blood samples (e.g., LTi) may aggravate the mycobacterial phenotype of *RORC*$^{-/-}$ patients.

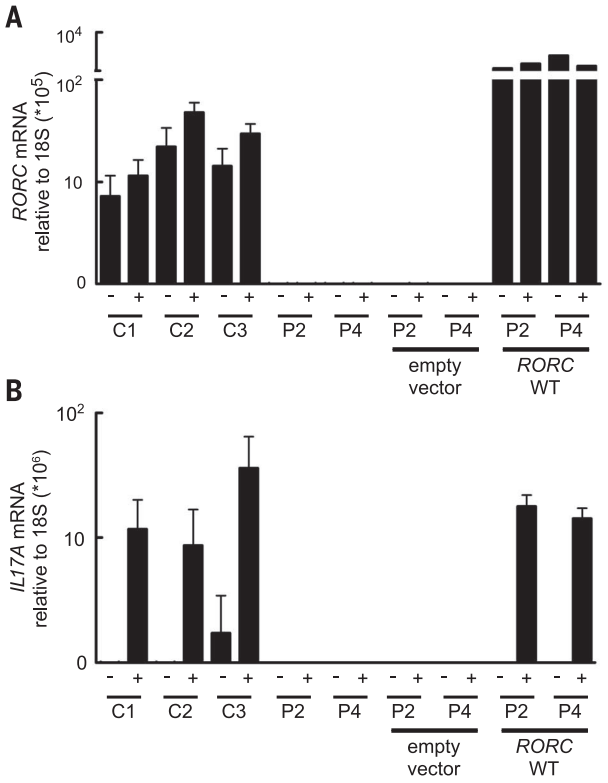

Fig. 4. T cell lines from *RORC*$^{-/-}$ patients fail to induce *IL17A* after mitogen stimulation. (**A**) *Herpesvirus saimiri*–transformed T cells from healthy donors (C1, C2, C3) or *RORC*$^{-/-}$ patients (P2, P4) were cultured in the presence (+) or absence (–) of PMA and ionomycin, and then total RNA was extracted and used for quantitative reverse transcription polymerase chain reaction for total *RORC*. T cell lines from *RORC*$^{-/-}$ patients were transduced with retrovirus encoding either a tag only (empty vector) or tagged WT *RORC* isoform 2. (**B**) *IL17A* expression was assessed in the same RNA samples presented in (A). *n* = 3 replicates; error bars represent SEM.

Conclusion

Collectively, these data demonstrate that human *RORC* plays a surprising dual role in host defense. These findings are clinically, immunologically, and genetically robust, as they were consistent in seven patients from three ethnic groups, homozygous for three different *RORC* mutations that are loss-of-function for both isoforms. Although the two infectious phenotypes are purely recessive, some immunological phenotypes showed codominant or dominant inheritance. The mild T cell lymphopenia, small thymus, lack of palpable axillary and cervical lymph nodes, and absence of MAIT and type 1 NKT cells in *RORC*$^{-/-}$ patients were consistent with the phenotype of *Rorc*$^{-/-}$ mice (table S3). Likewise, impaired IL-17A/F immunity was predicted to account for impaired protection against *Candida albicans* (*35*), as *Rorc* is the master gene controlling T$_H$17 differentiation in inbred mice (*11*), and mutations affecting human IL-17A/F immunity underlie isolated CMC (*1*, *26*, *36*). The IL-17A/F defect therefore underlies CMC in RORγT-deficient patients, probably but not necessarily because of T cells, as other cells can produce these cytokines in healthy individuals. We expected these patients to be susceptible to candidiasis, but their susceptibility to mycobacterial disease and its severity were unanticipated. This phenotype does not seem to be human-specific, as we also found that mice deficient for *Rorc* (*14*) are susceptible to mycobacterial infection (fig. S19). Our data conclusively demonstrate that human *RORC* plays an indispensable role in the induction of IFN-γ–dependent antimycobacterial systemic immunity. The mechanism underlying disease in these patients probably involves an impairment of the induction of IFN-γ production by γδ T cells, CCR6$^+$CXCR3$^+$CD4$^+$ αβ T$_H$1* cells, or both in response to mycobacteria. Other mechanisms may also be at work. Human *RORC* is essential not only for the development of IL-17A/F–producing lymphocytes protecting the mucocutaneous barriers against *Candida* but also for the activation of IFN-γ–producing T cells and for systemic protection against *Mycobacterium*.

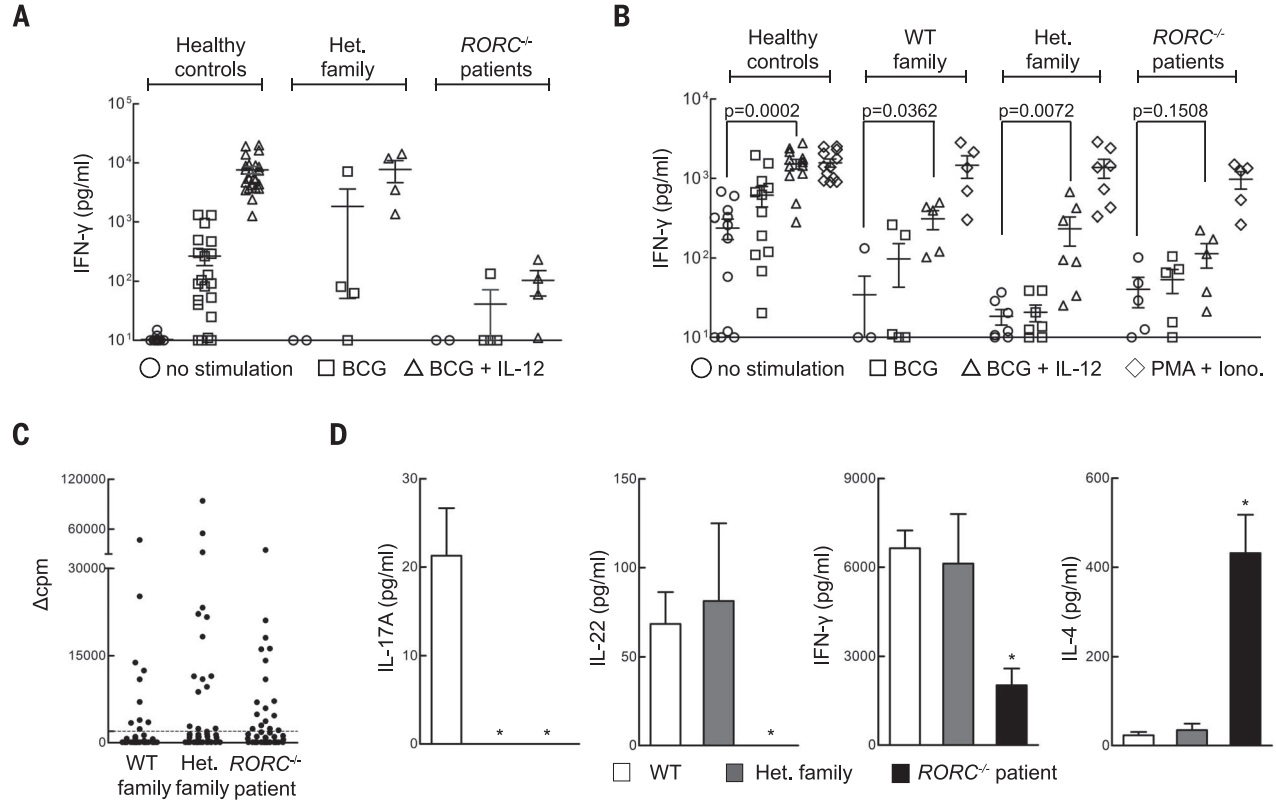

Fig. 5. Cellular mechanisms of impaired IFN-γ immunity to *Mycobacterium* in *RORC*$^{-/-}$ patients. (**A**) Whole-blood samples from healthy controls (n = 23), heterozygous family members (n = 4), or *RORC*$^{-/-}$ patients (n = 4) were incubated for 48 hours under three different sets of activation conditions: (i) medium alone, (ii) live *M. bovis*–BCG (BCG) at a multiplicity of infection of 20 BCG cells per leukocyte, and (iii) BCG plus 20 ng/ml IL-12. The IFN-γ levels of culture supernatants were determined by enzyme-linked immunosorbent assay (ELISA). (**B**) Equal numbers of live PBMCs from healthy controls, WT family members, heterozygous family members, or *RORC*$^{-/-}$ patients were cultured in the presence of live BCG, BCG and IL-12, or PMA/ionomycin for 48 hours. IFN-γ concentration in the culture supernatant was assessed by ELISA. (**C**) Sorted CCR6^{+} memory CD4^{+} T cells were polyclonally stimulated with PHA in the presence of irradiated allogeneic feeder cells and IL-2 to generate T cell libraries, as in Fig. 3D. Library screening was performed 14 to 21 days after initial stimulation by culturing thoroughly washed T cells with autologous irradiated B cells, with or without a 3-hour pulse with *M. bovis*–BCG peptide pools. Proliferation was measured by radiolabel incorporation on day 4 and is expressed as Δcpm values. Each symbol illustrates one culture. Dotted lines represent the cutoff value. The frequencies of specific T cells calculated using the Poisson distribution were 467/10^{6}, 749/10^{6}, and 875/10^{6} in WT control, heterozygous family member, and *RORC*$^{-/-}$ patient, respectively. (**D**) The cytokines indicated were determined in the culture supernatants from (C) for wells with Δcpm values above the cutoff value. Number of wells: n = 45 to 64 for WT controls, n = 4 to 10 for heterozygous family members, and n = 14 to 23 for *RORC*$^{-/-}$ patients. *P < 0.05 versus WT controls; in two-tailed Mann-Whitney tests with Bonferroni correction. Error bars in (D) indicate SEM.

REFERENCES AND NOTES

1. A. Puel *et al.*, *Science* **332**, 65–68 (2011).
2. Y. Ling *et al.*, *J. Exp. Med.* **212**, 619–631 (2015).
3. D. Bogunovic *et al.*, *Science* **337**, 1684–1688 (2012).
4. J. Bustamante, S. Boisson-Dupuis, L. Abel, J.-L. Casanova, *Semin. Immunol.* **26**, 454–470 (2014).
5. M. Kircher *et al.*, *Nat. Genet.* **46**, 310–315 (2014).
6. A. Medvedev, A. Chistokhina, T. Hirose, A. M. Jetten, *Genomics* **46**, 93–102 (1997).
7. I. Villey, R. de Chasseval, J. P. de Villartay, *Eur. J. Immunol.* **29**, 4072–4080 (1999).
8. Y. W. He, M. L. Deftos, E. W. Ojala, M. J. Bevan, *Immunity* **9**, 797–806 (1998).
9. Q. Ruan *et al.*, *J. Exp. Med.* **208**, 2321–2333 (2011).
10. G. Eberl, D. R. Littman, *Immunol. Rev.* **195**, 81–90 (2003).
11. I. I. Ivanov *et al.*, *Cell* **126**, 1121–1133 (2006).
12. J. Guo *et al.*, *Nat. Immunol.* **3**, 469–476 (2002).
13. X. O. Yang *et al.*, *Immunity* **28**, 29–39 (2008).
14. G. Eberl *et al.*, *Nat. Immunol.* **5**, 64–73 (2004).
15. C. E. Sutton *et al.*, *Immunity* **31**, 331–341 (2009).
16. M. L. Robinette *et al.*, *Nat. Immunol.* **16**, 306–317 (2015).
17. M. L. Michel *et al.*, *Proc. Natl. Acad. Sci. U.S.A.* **105**, 19845–19850 (2008).
18. T. Egawa *et al.*, *Immunity* **22**, 705–716 (2005).
19. D. F. Hoft, R. M. Brown, S. T. Roodman, *J. Immunol.* **161**, 1045–1054 (1998).
20. I. Van Rhijn *et al.*, *Nat. Immunol.* **14**, 706–713 (2013).
21. L. D. Notarangelo, *Annu. Rev. Immunol.* **31**, 195–225 (2013).
22. Z. Sun *et al.*, *Science* **288**, 2369–2373 (2000).
23. G. Eberl, D. R. Littman, *Science* **305**, 248–251 (2004).
24. H. Takatori *et al.*, *J. Exp. Med.* **206**, 35–41 (2009).
25. E. V. Acosta-Rodriguez *et al.*, *Nat. Immunol.* **8**, 639–646 (2007).
26. B. Boisson *et al.*, *Immunity* **39**, 676–686 (2013).
27. J. Feinberg *et al.*, *Eur. J. Immunol.* **34**, 3276–3284 (2004).
28. M. Ouederni *et al.*, *Blood* **118**, 5108–5118 (2011).
29. O. de la Calle-Martin *et al.*, *J. Clin. Invest.* **108**, 117–123 (2001).
30. B. Pasquier *et al.*, *J. Exp. Med.* **201**, 695–701 (2005).
31. E. Martin *et al.*, *Nature* **510**, 288–292 (2014).
32. A. C. Chan *et al.*, *Science* **264**, 1599–1601 (1994).
33. N. V. Morgan *et al.*, *J. Clin. Invest.* **121**, 695–702 (2011).
34. L. Le Bourhis *et al.*, *Nat. Immunol.* **11**, 701–708 (2010).
35. H. R. Conti *et al.*, *J. Exp. Med.* **206**, 299–311 (2009).
36. L. Liu *et al.*, *J. Exp. Med.* **208**, 1635–1648 (2011).
37. Materials and methods are available as supplementary materials on *Science* Online.

ACKNOWLEDGMENTS

We thank the patients and their families for their collaboration; both branches of the Laboratory of Human Genetics of Infectious Diseases for helpful discussions and support; M. Hindiyeh for expert clinical care of the patients from Kindred A; G. C. Tsokos for providing the *IL17A* reporter luciferase plasmid; E. Van de Vosse for providing the pLZRS-IRES-ΔNGFR vector; D. Littman for helpful discussions; B. Fleckenstein and M. Schmidt for the generation of patient-derived T cell lines; and Y. Nemirovskaya, L. Amar, E. Anderson, M. Courat, and T. Nivare for administrative support. The data presented in the manuscript are tabulated in the main paper and in the supplementary materials. The sequence data are available in the Sequence Read Archive (www.ncbi.nlm.nih.gov/sra) with accession numbers SRS964935, SRS965039, SRS965040, and SRS965042. J.Mc. and The University of Melbourne filed Australian provisional patent application numbers 2014901185 and 2014901 that relate to ligands that bind MR1 and stimulate MAIT cells. The Laboratory of Human Genetics of Infectious Diseases is supported by grants from the National Center for Research Resources and the National Center for Advancing Sciences,

NIH (8UL1TR000043); the French National Research Agency (ANR) under the "Investments for the Future" program (grant ANR-10-IAHU-01), grant IFNGPHOX (13-ISV3-0001-01 to J.B.), and grant GENCMCD (11-BSV3-005-01 to A.P); Laboratoire d'Excellence Integrative Biology of Emerging Infectious Diseases (ANR-10-LABX-62-IBEID); the National Health and Medical Research Council (NHMRC) (to E.K.D., C.S.M., S.G.T, and J.Mc.); the Rockefeller University; INSERM; Université Paris Descartes; the St. Giles Foundation; the National Institute of Allergy and Infectious Diseases (R37AI095983 to J.-L.C.); and the NIH (contract HHSN272200900044C to A.S.). S.O. was supported by Grants-in-Aid for Scientific Research from the Japan Society for the Promotion of Science (25713039 and 25670477), J.G.M. by the Canadian Institutes of Health Research, R.M.-B. by the European Molecular Biology Organization, Y.I. by the AXA Research Fund, L.A.H. by the Rheumatology Research Foundation's Scientist Development Award, and F.S. by grants from the European Research Council (323183 PREDICT) and the Swiss National Science Foundation (149475). The Institute for Research in Biomedicine and the Center of Medical Immunology are supported by the Helmut Horten Foundation. S.A.-M. is the bronchial asthma research chair of the Prince Naif Center for Immunology Research.

SUPPLEMENTARY MATERIALS

www.sciencemag.org/content/349/6248/606/suppl/DC1
Materials and Methods
Supplementary Text
Figs. S1 to S19
Tables S1 to S3
References (*38*–*67*)

7 December 2014; accepted 29 June 2015
Published online 9 July 2015
10.1126/science.aaa4282

TOPOLOGICAL MATTER

Discovery of a Weyl fermion semimetal and topological Fermi arcs

Su-Yang Xu,[1,2]* Ilya Belopolski,[1]* Nasser Alidoust,[1,2]* Madhab Neupane,[1,3]* Guang Bian,[1] Chenglong Zhang,[4] Raman Sankar,[5] Guoqing Chang,[6,7] Zhujun Yuan,[4] Chi-Cheng Lee,[6,7] Shin-Ming Huang,[6,7] Hao Zheng,[1] Jie Ma,[8] Daniel S. Sanchez,[1] BaoKai Wang,[6,7,9] Arun Bansil,[9] Fangcheng Chou,[5] Pavel P. Shibayev,[1,10] Hsin Lin,[6,7] Shuang Jia,[4,11] M. Zahid Hasan[1,2]†

A Weyl semimetal is a new state of matter that hosts Weyl fermions as emergent quasiparticles and admits a topological classification that protects Fermi arc surface states on the boundary of a bulk sample. This unusual electronic structure has deep analogies with particle physics and leads to unique topological properties. We report the experimental discovery of a Weyl semimetal, tantalum arsenide (TaAs). Using photoemission spectroscopy, we directly observe Fermi arcs on the surface, as well as the Weyl fermion cones and Weyl nodes in the bulk of TaAs single crystals. We find that Fermi arcs terminate on the Weyl fermion nodes, consistent with their topological character. Our work opens the field for the experimental study of Weyl fermions in physics and materials science.

Weyl fermions have long been known in quantum field theory, but have not been observed as a fundamental particle in nature (*1*–*3*). Recently, it was understood that a Weyl fermion can emerge as a quasiparticle in certain crystals, Weyl fermion semimetals (*1*–*22*). Despite being a gapless metal, a Weyl semimetal is characterized by topological invariants, broadening the classification of topological phases of matter beyond insulators. Specifically, Weyl fermions at zero energy correspond to points of bulk band degeneracy, Weyl nodes, which are associated with a chiral charge that protects gapless surface states on the boundary of a bulk sample. These surface states take the form of Fermi arcs connecting the projection of bulk Weyl nodes in the surface Brillouin zone (BZ) (*6*). A band structure like the Fermi arc surface states would violate basic band theory in an isolated two-dimensional (2D) system and can only arise on the boundary of a 3D sample, providing a dramatic example of the bulk-boundary correspondence in a topological phase. In contrast to topological insulators where only the surface states are interesting (*21*, *22*), a Weyl semimetal features unusual band structure in the bulk and on the surface. The Weyl fermions in the bulk are predicted to provide a condensed-matter realization of the chiral anomaly, giving rise to a negative magnetoresistance under parallel electric and magnetic fields, unusual optical conductivity, nonlocal transport, and local nonconservation of ordinary current (*5*, *12*–*16*). At the same time, the Fermi arc surface states are predicted to show unconventional quantum oscillations in magneto-transport, as well as unusual quantum interference effects in tunneling spectroscopy (*17*–*19*). The prospect of the realization of these phenomena has inspired much experimental and theoretical work (*1*–*22*).

Here we report the experimental realization of a Weyl semimetal in a single crystalline material, tantalum arsenide (TaAs). Using the combination of the vacuum ultraviolet (low–photon-energy) and soft x-ray (SX) angle-resolved photoemission spectroscopy (ARPES), we systematically and differentially study the surface and bulk electronic structure of TaAs. Our ultraviolet (low–photon-energy) ARPES measurements, which are highly surface sensitive, demonstrate the existence of the Fermi arc surface states, consistent with our band calculations presented here. Moreover, our SX-ARPES measurements, which are reasonably bulk sensitive, reveal the 3D linearly dispersive bulk Weyl cones and Weyl nodes. Furthermore, by combining the low–photon-energy and SX-ARPES data, we show that the locations of the projected bulk Weyl nodes correspond to the terminations of the Fermi arcs within our experimental resolution. These systematic measurements demonstrate TaAs as a Weyl semimetal.

The material system and theoretical considerations

Tantalum arsenide is a semimetallic material that crystallizes in a body-centered tetragonal lattice system (Fig. 1A) (*23*). The lattice constants are a = 3.437 Å and c = 11.656 Å, and the space group is $I4_1md$ (#109, C_{4v}), as consistently reported in previous structural studies (*23*–*25*). The crystal consists of interpenetrating Ta and As sublattices, where the two sublattices are shifted by $(\frac{a}{2}, \frac{a}{2}, \delta)$, $\delta \approx \frac{c}{12}$. Our diffraction data match well with the lattice parameters and the space group $I4_1md$ (*26*). The scanning tunneling microscopic (STM) topography (Fig. 1B) clearly resolves the (001) square lattice without any obvious defect. From the topography, we obtain a lattice constant a = 3.45 Å. Electrical transport measurements on TaAs confirmed its semimetallic transport properties and reported negative magnetoresistance, suggesting the anomalies due to Weyl fermions (*23*).

We discuss the essential aspects of the theoretically calculated bulk band structure (*9*, *10*) that predicts TaAs as a Weyl semimetal candidate. Without spin-orbit coupling, calculations (*9*, *10*) show that the conduction and valence bands interpenetrate (dip into) each other to form four 1D line nodes (closed loops) located on the k_x and k_y planes (shaded blue in Fig. 1, C and E). Upon the inclusion of spin-orbit coupling, each line node loop is gapped out and shrinks into six Weyl nodes that are away from the $k_x = 0$ and $k_y = 0$ mirror planes (Fig. 1E, small filled circles). In our calculation, in total there are 24 bulk Weyl cones (*9*, *10*), all of which are linearly dispersive and are associated

[1]Laboratory for Topological Quantum Matter and Spectroscopy (B7), Department of Physics, Princeton University, Princeton, NJ 08544, USA. [2]Princeton Center for Complex Materials, Princeton Institute for Science and Technology of Materials, Princeton University, Princeton, NJ 08544, USA. [3]Condensed Matter and Magnet Science Group, Los Alamos National Laboratory, Los Alamos, NM 87545, USA. [4]International Center for Quantum Materials, School of Physics, Peking University, China. [5]Center for Condensed Matter Sciences, National Taiwan University, Taipei 10617, Taiwan. [6]Centre for Advanced 2D Materials and Graphene Research Centre National University of Singapore, 6 Science Drive 2, Singapore 117546. [7]Department of Physics, National University of Singapore, 2 Science Drive 3, Singapore 117542. [8]Quantum Condensed Matter Division, Oak Ridge National Laboratory, Oak Ridge, TN 37831, USA. [9]Department of Physics, Northeastern University, Boston, MA 02115, USA. [10]Princeton Institute for Science and Technology of Materials, Princeton University, Princeton, NJ 08544, USA. [11]Collaborative Innovation Center of Quantum Matter, Beijing, 100871, China.
*These authors contributed equally to this work. †Corresponding author. E-mail: mzhasan@princeton.edu

Impairment of immunity to *Candida* and *Mycobacterium* in humans with bi-allelic *RORC* mutations

Satoshi Okada *et al.*

Science **349**, 606 (2015);
DOI: 10.1126/science.aaa4282